Kendall M. Jones, MD • Robert V. Mulkern, PhD • Michael T. Mantello, MD • Phillipe S. Melki, MD
Sungkee S. Ahn, MD • Patrick D. Barnes, MD • Ferenc A. Jolesz, MD

Brain Hemorrhage: Evaluation with Fast Spin-Echo and Conventional Dual Spin-Echo Images[1]

Signal intensity of blood products on proton-density– and T2-weighted images obtained with spin-echo (SE) and fast SE (FSE) sequences was evaluated in 15 patients with central nervous system hemorrhage to determine the extent of differences between the two techniques when signal loss from magnetic susceptibility effects in hemorrhagic lesions is considered. Within operator-defined regions of interest, signal intensity of hemorrhage, iron-containing nuclei, white matter, scalp fat, and noise was measured along the phase-encoding direction. Hemosiderin, deoxyhemoglobin, and iron-containing nuclei had slightly higher signal intensity on FSE images than on SE images, but the differences were not statistically significant. Signal intensity of methemoglobin was similar with both sequences, whereas that of scalp fat was higher on FSE images. Signal intensity measurements for most tissues studied were comparable, but the signal-to-noise ratios with FSE imaging were less than those with SE imaging. Although paramagnetic blood products may show slightly higher signal intensity with FSE imaging, contrast with the two sequences was comparable and lesion conspicuity was nearly identical.

Index terms: Blood, MR • Brain, hemorrhage, 10.367, 10.782 • Magnetic resonance (MR), comparative studies • Magnetic resonance (MR), experimental • Magnetic resonance, (MR), rapid imaging

Radiology 1992; 182:53–58

[1] From the Department of Radiology, Brigham and Women's Hospital, Harvard Medical School, 75 Francis St, Boston, MA 02115 (K.M.J., M.T.M., P.S.M., S.S.A., F.A.J.), and the Department of Radiology, Children's Hospital, Boston (R.V.M., P.D.B.). From the 1991 RSNA scientific assembly. Received June 21, 1991; revision requested July 17; revision received August 7; accepted August 16. **Address reprint requests to** K.M.J.

THE detection of intracranial hemorrhage is of critical importance in patient management due to the frequent necessity of neurosurgical intervention in these patients. The appearance and conspicuity of various blood products are therefore important in the evaluation of alternative rapid pulse sequences.

Fast spin-echo (FSE) magnetic resonance (MR) imaging is a relatively new technique that can be used for rapid acquisition of proton-density (PD)– and T2-weighted images (1–3). Dual-contrast images of the entire brain at 14 section locations may be obtained in 2–3 minutes with FSE imaging. The use of many closely spaced 180° pulses can theoretically reduce contributions from various T2 decay mechanisms, including spin-spin coupling interactions among lipid protons (4,5) and diffusion of water through local, susceptibility-induced, microscopic field gradients (6–8). Because of the latter effect, it may be argued that FSE imaging may be less sensitive to magnetic susceptibility signal loss than are conventional SE methods that use larger echo spacings. Our study was undertaken to determine if there are measurable differences between the two techniques when signal intensities from hemorrhagic lesions—in which magnetic susceptibility effects play an important role in image contrast—are considered.

MATERIALS AND METHODS

Dual-contrast FSE sequences based on rapid acquisition with repeated echo sequences (1,2) and modified with a specific phase-encoding reordering algorithm described elsewhere were used (3). The algorithm allows for convenient T2 contrast manipulation through operator-chosen pseudo-echo times (pTEs), which are analogous to conventional echo times (TEs) used with SE sequences. The dual FSE sequence we used consisted of repeated applications of an eight-echo Carr-Purcell-Meiboom-Gill train. The echo spacings in the train were between 15 and 18 msec. The first four echoes of each train were used to acquire four k-space (9) data lines for the PD-weighted image, while the next four echoes were used to acquire four k-space data lines for the T2-weighted image. With this sequence, 256 phase-encoding steps may be acquired in only 64 repetition times (TR). Acquisition of the same number of phase-encoding steps with conventional SE methods requires a time period of 256 TR. Thus, the dual-contrast FSE sequence leads to a theoretical reduction in imaging time by a factor of 4. Because the effective echo train lengths in FSE imaging are approximately 130 msec, however, fewer sections can be accessed per TR interval than with conventional SE sequences. The practical reduction in the actual time/image ratio of dual FSE imaging over SE imaging is closer to a factor of 3 when identical matrix sizes and number of section locations are considered.

Patients

A total of 15 patients aged 5 months to 81 years (mean age, 31 years; eight adults and seven children) were evaluated with FSE imaging immediately after undergoing conventional SE imaging. The study was performed over a 4-month period. Patients were included on the basis of hemorrhage seen on computed tomographic (CT) scans or on initial conventional SE images.

Categorization of Blood Products

Blood products were categorized according to the appearance of the lesions on T1-weighted, PD- and T2-weighted SE images, clinical history, appearance on CT scans, and appearance on previous MR images. When present, the appearance of an inner or outer core provided additional information for categorization. Blood products were broadly classified into cate-

Abbreviations: FSE = fast spin echo, PD = proton density, pTE = pseudo-echo time, RF = radio frequency, ROI = region of interest, SE = spin echo, S/N = signal-to-noise ratio, TE = echo time, TR = repetition time.

gories of deoxyhemoglobin (generally isointense to low signal intensity on T1-weighted images and low intensity on T2-weighted images), methemoglobin (high intensity on T1- and T2-weighted images), and hemosiderin (very low signal intensity on T1- and T2-weighted images). With these criteria, 17 foci of methemoglobin, 11 foci of hemosiderin, and four foci of deoxyhemoglobin were identified on the routine SE images obtained in the 15 patients.

SE and FSE Imaging Parameters

The SE imaging protocol included obtainment of scout sagittal T1-weighted (600/18 [TR msec/TE msec]) images. In seven patients, this was followed by conventional PD- and T2-weighted imaging performed with two signal averages, a 256 × 128 matrix, and a 5-mm section thickness with a 2.5-mm gap (total acquisition time, 8 minutes and 56 seconds for 18 sections). In eight patients, a half-Fourier SE sequence was performed by using a 256 × 192 matrix. Two serial acquisitions with this sequence, to image the entire brain with 32 contiguous 5-mm sections, required 7 minutes and 40 seconds of imaging time.

The FSE sequences consisted of a 256 × 128 matrix, two signal averages, and imaging time of 2 minutes and 8 seconds (three patients); a 256 × 192 matrix, two signal averages, and imaging time of 3 minutes and 12 seconds (four patients); a 256 × 192 matrix, one signal average, and time of 1 minute and 36 seconds (two patients); or a 256 × 256 matrix, one signal average, and time of 2 minutes and 8 seconds (six patients). In all FSE sequences, 14 sections 5 mm long with a 2.5-mm intersection gap were acquired. All FSE echoes were collected with a 16-kHz bandwidth, as were the echoes used for the SE PD-weighted images. An 8-kHz bandwidth was employed for the second echo of the conventional SE sequences.

The TRs of the conventional SE sequences and the dual-contrast FSE sequences were matched at 2,000 msec. The TEs of the SE sequences were 30 and 80 msec. In 12 of 15 cases, the pTEs of the FSE sequences were 15 and 90 msec; in three cases, pTEs were 30 and 90 msec.

Signal Intensity and Signal-to-Noise (S/N) Measurements

Within operator-defined regions of interest (ROIs), signal intensity measurements were obtained from the hemorrhagic foci identified on both types of images. Signal intensity of identical regions was measured on PD- and T2-weighted images for each pulse sequence. ROIs in conventional SE and FSE image data sets were matched as closely as possible. Multiple measurements were obtained within most hemorrhagic foci due to the complex nature of the blood products; for example, a single area of hemorrhage might show signal characteristics of deoxyhemoglobin centrally with a high-intensity surrounding rim of methemoglobin. Additional signal intensity measurements were obtained from ROIs in white matter and scalp fat, and noise was measured in large ROIs outside of the head but along the phase-encoding direction. In the adult patients, signal intensity measurements for iron-containing nuclei of the dentate nucleus, globus pallidus, and substantia nigra were also obtained. Observations concerning overall image quality, artifacts, and lesion conspicuity were recorded.

Correlation plots between FSE and SE signal intensities were made for each tissue sampled to determine how signal intensity characteristics compared under the imaging conditions described. An automatic prescanning procedure, which sets the receive and transmit gains, was performed prior to every data acquisition. Phantom studies have revealed that when this procedure is performed prior to each acquisition of a given sequence, changes in matrix size and number of signal averages result in less than a 5% change in the signal intensities. The noise values along the readout gradient direction, however, accurately reflect the standard changes in S/N with respect to matrix size and number of signal averages (10). Signal intensity measurements from FSE and SE images therefore should reveal differences in contrast even when they are acquired with different matrix sizes or number of signal averages, and correction factors when identical TEs or pTEs and TRs are used should be unnecessary. When S/N values were evaluated, however, the appropriate correction factors were applied to account for differences in matrix size and number of signal averages, thus allowing comparison of the inherent S/N values of each sequence. Only measurements of noise outside the imaged object and along the phase-encoding direction were used, since these are said to offer a more "valid measure for comparison purposes if one is interested in assessing the impact of various techniques on image quality . . ." (10).

Statistical Analysis

Statistical analyses included calculation of means and standard deviations of signal intensity and corrected S/N values for each tissue from each type of sequence. Paired *t* tests were performed to determine the statistical significance of differences between signal intensities and S/N values obtained with the FSE and SE sequences. In 12 of 15 cases, the pTE was 15 msec for PD-weighted FSE images and 30 msec for PD-weighted SE images. In all cases, the T2-weighted FSE images utilized 90 msec, versus 80 msec for the SE T2-weighted images. To estimate the importance of these differences, the mean signal intensity values from both "echoes" of the FSE sequences were used to extrapolate mean signal intensities anticipated at 30-msec and 80-msec pTEs, which were used throughout for the SE sequences. The equation used for this purpose was

$$S_3 = S_1(S_1/S_2)[(TE_1 - TE_3)/(TE_2 - TE_1)] \quad (1)$$

where S_3 is the extrapolated signal intensity at TE_3 obtained from the measured signal intensities S_1 and S_2 acquired at TE_1 and TE_2. The equation is derived by assuming that signal intensity S_i at echo time TE_i (i = 1, 2, or 3) is proportional to $M_0\exp(-TE_i/T2)$, where M_0 is the transverse magnetization following the 90° pulse.

RESULTS

Correlation between signal intensities measured on FSE images versus those measured on SE images for lesions characterized as methemoglobin, hemosiderin, and deoxyhemoglobin and for white matter, subcutaneous fat, and iron-containing nuclei was rather strong (Figs 1, 2). Correlation coefficients for eight of the 12 plots (six tissues, PD- and T2-weighted image comparisons) were above .88. The T2-weighted methemoglobin plot had a correlation coefficient of .61, the T2-weighted fat plot had a correlation coefficient of .82, and the PD- and T2-weighted iron-containing nuclei plots had correlation coefficients of .78 and .63, respectively. For hemosiderin, deoxyhemoglobin, and iron-containing nuclei on FSE images, slightly less signal loss due to magnetic susceptibility effects may result; more points above than below the perfect correlation diagonal line are evidence of this (Figs 1b, 1c, 2c). As reported previously (3), scalp fat appears to have significantly higher intensity with both echoes on FSE images than on SE images, which is supported by the correlation plot in Figure 2b. Signal intensity of cerebral white matter tends to be less on FSE images than on SE images (Fig 2a).

Table 1 lists the means and standard deviations of the signal intensities of the various tissues on PD- and T2-weighted FSE and SE images. A trend toward higher signal intensities on FSE images for all tissues except white matter is demonstrated. Direct comparisons between SE and FSE PD-weighted studies, as well as between SE and FSE T2-weighted studies, however, reveal that this trend is not of any statistical significance ($P > .2$), except in the case of fat ($P < .001$). The extrapolated mean signal intensities (calculated with Eq [1]) for the FSE PD- and T2-weighted images if pTEs of 30 msec and 80 msec had been used are listed below the respective measured values in Table 1. In the case of the PD-weighted images, the extrapolation to 30-msec pTEs

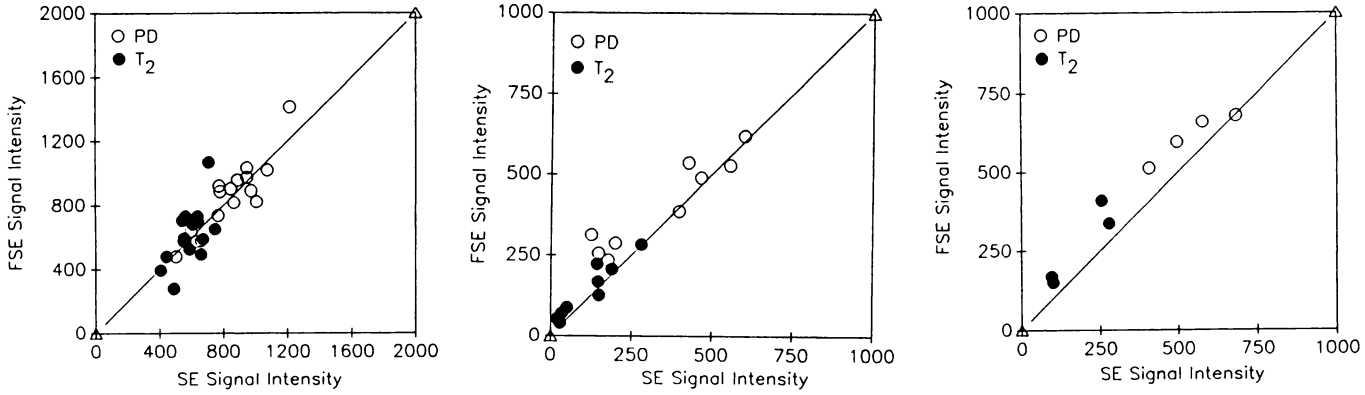

a. b. c.

Figure 1. FSE versus SE signal intensity correlation plots for **(a)** methemoglobin, **(b)** hemosiderin, and **(c)** deoxyhemoglobin. ○ = measurements from PD-weighted images, ● = measurements from T2-weighted images.

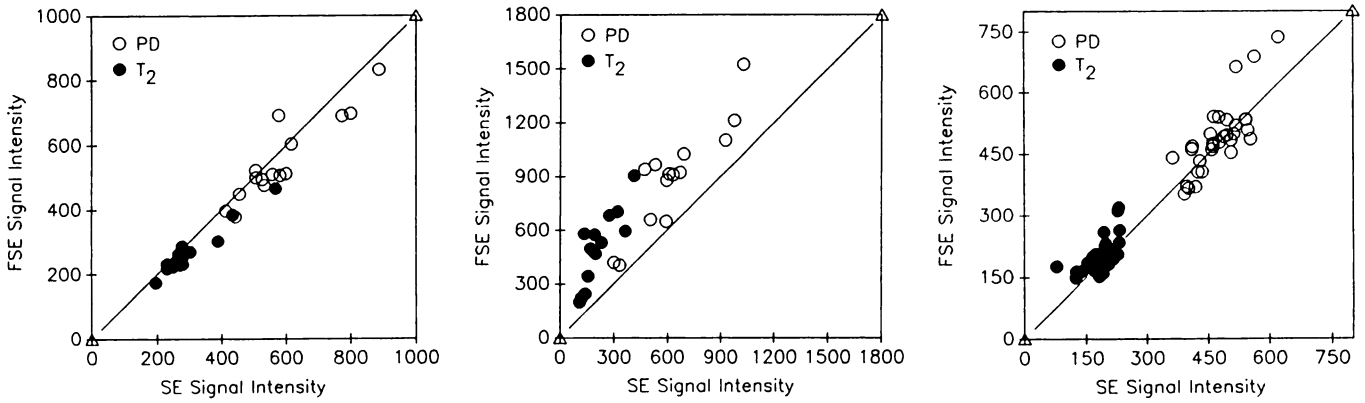

a. b. c.

Figure 2. FSE versus SE signal intensity correlation plots for **(a)** white matter, **(b)** subcutaneous fat, and **(c)** iron-containing nuclei. ○ = measurements from PD-weighted images, ● = measurements from T2-weighted images.

Table 1
Means and Standard Deviations of Signal Intensities of Blood Products and Tissues on SE and FSE MR Images

Blood Products and Tissues	No. of Measurements	PD weighted		T2 weighted	
		SE	FSE	SE	FSE
Methemoglobin	13	842 ± 187	853 ± 226 800	585 ± 279	619 ± 647
Hemosiderin	9	344 ± 183	405 ± 141 328	116 ± 88	140 ± 162
Deoxyhemoglobin	4	540 ± 117	612 ± 75 518	182 ± 97	267 ± 297
White matter	15	579 ± 129	545 ± 119 472	297 ± 89	266 ± 293
Scalp fat	15	630 ± 206	908 ± 279 808	209 ± 89	506 ± 547
Iron-containing nuclei	28	478 ± 56	489 ± 81 411	185 ± 33	203 ± 228

Note.—Extrapolated values for 30-msec and 80-msec pTEs determined with Equation (1) are listed below the measured values for the PD-weighted FSE results.

predicts that signal intensities with FSE sequences would be slightly lower than with SE sequences, although the differences would be insignificant except for fat. The use of an 80-msec pTE rather than a 90-msec pTE, however, would serve to enhance the observed signal intensity gains of FSE over SE sequences with regard to the paramagnetic blood products. The 6% increase in mean signal intensity for methemoglobin would approach 10%, the 20% mean signal intensity increase for hemosiderin would approach 40%, and the observed 46% mean signal intensity increase for deoxyhemoglobin would approach 63%.

The FSE images generally contained more noise along the phase-encoding axis than did the SE images, even when corrections for matrix size and number of signal averages were accounted for. Since the signal intensities were largely correlated for all tissues except fat, S/N values for FSE images were reduced when compared with those on SE images. Table 2 lists the means and standard deviations of the S/N values for SE and FSE PD- and T2-weighted images for all tissues studied. For every tissue but fat, S/N values are lower for FSE than for SE images. Among the PD-weighted images, statistically significant lower S/N values are found for white matter and iron-containing nuclei on FSE images ($P < .05$). When the T2-weighted images are considered, significantly lower S/N values are found for methemoglobin as well as for white matter and iron-containing nuclei on FSE images ($P < .05$).

Visual impressions confirm the trend observed in Table 1. The appearance of deoxyhemoglobin, hemosiderin, and iron-containing nuclei was slightly less intense on conventional SE images than on the corresponding FSE images (Figs 3–6). Methemoglobin appears equally intense on FSE and SE images (Figs 3, 4), and fat is markedly more intense on FSE images (Figs 3b, 4b). In several cases, reduced motion artifact was observed on FSE images, which would be expected with the shorter acquisition times. In all cases, FSE images were of diagnostic quality and, compared with SE images, had nearly identical lesion conspicuity and comparable overall image quality.

Table 2
Means and Standard Deviations of S/N of Blood Products and Tissues on SE and FSE MR Images

Blood Products and Tissues	No. of Measurements	PD weighted		T2 weighted	
		SE	FSE	SE	FSE
Methemoglobin	13	76 ± 23	61 ± 29	75 ± 17	46 ± 17
Hemosiderin	9	31 ± 18	24 ± 9	16 ± 11	9 ± 5
Deoxyhemoglobin	4	53 ± 21	43 ± 10	25 ± 17	20 ± 10
White matter	15	51 ± 14	35 ± 9	34 ± 11	18 ± 4
Scalp fat	15	52 ± 19	54 ± 16	25 ± 10	32 ± 12
Iron-containing nuclei	28	45 ± 13	32 ± 8	24 ± 9	15 ± 4

Note.—Noise values were normalized to account for different matrix sizes and number of signal averages.

DISCUSSION

The desire to decrease MR imaging time, increase patient volume, and improve image quality has led to the development of multiple fast pulse sequences. The FSE sequence is based on partial radio-frequency (RF) echo planar methods (1–3) with a specific phase-encoding reordering algorithm (3). Because of the use of RF spin echoes rather than gradient-recalled echoes, FSE images demonstrate pronounced "SE-like" contrast. It has been suggested that, due to the use of many closely spaced RF refocusing pulses, FSE images would demonstrate less sensitivity to magnetic susceptibility effects than would conventional SE images (3). The 1.4-T in vitro findings of Gomori et al (8), in which the T2 of some blood products varied substantially as echo spacings ranged from 2 to 64 msec, also suggest that FSE and conventional SE images may show differences for hemorrhagic lesions.

Our 1.5-T in vivo study does not demonstrate the relatively large differences in signal intensity from blood products at SE and FSE imaging that the in vitro study of Gomori et al suggested (8). The data showed slightly less signal loss due to magnetic susceptibility effects on FSE images, which is evident from the trend toward slightly higher signal intensity from deoxyhemoglobin, hemosiderin, and iron-containing nuclei. As seen in Figures 3–6, these areas appeared slightly less dark with both echoes of the FSE sequence. On neither the PD nor T2-weighted images, however, were these findings statistically significant for any of the three categories of blood products ($P > .2$), although the use of 80-msec rather than 90-msec pTEs would have increased the differ-

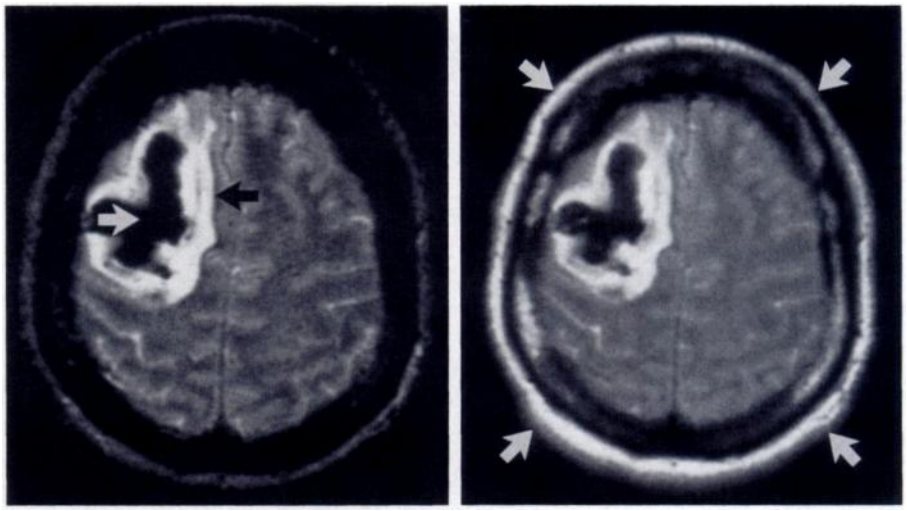

a. b.

Figure 3. **(a)** Conventional SE T2-weighted image (2,000/80) shows hemorrhage in right side of brain with low-intensity central deoxyhemoglobin (white arrow) and high-intensity surrounding rim of methemoglobin (black arrow) that was also hyperintense on T1-weighted SE image (not shown). **(b)** FSE image (2,000/pTE, 80) shows slightly greater signal intensity in central deoxyhemoglobin, whereas signal intensity of methemoglobin is similar to that on SE images. Quantitative measurements of signal intensity confirmed these visual impressions. Scalp fat has very high signal intensity (arrows).

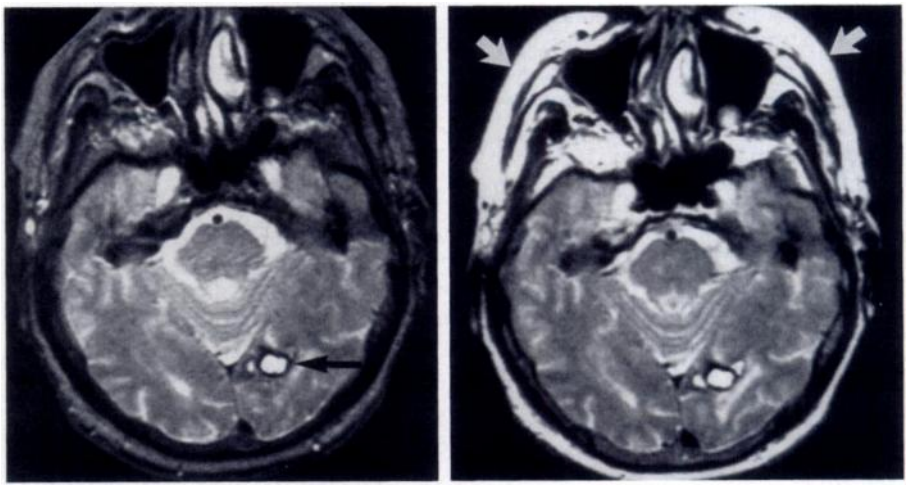

a. b.

Figure 4. **(a)** Conventional T2-weighted SE image (2,000/80) shows left occipital hemorrhage with central methemoglobin and surrounding hemosiderin ring (arrow). **(b)** Signal of hemosiderin ring appears slightly more intense on FSE image. Fat again has very high signal intensity (arrows).

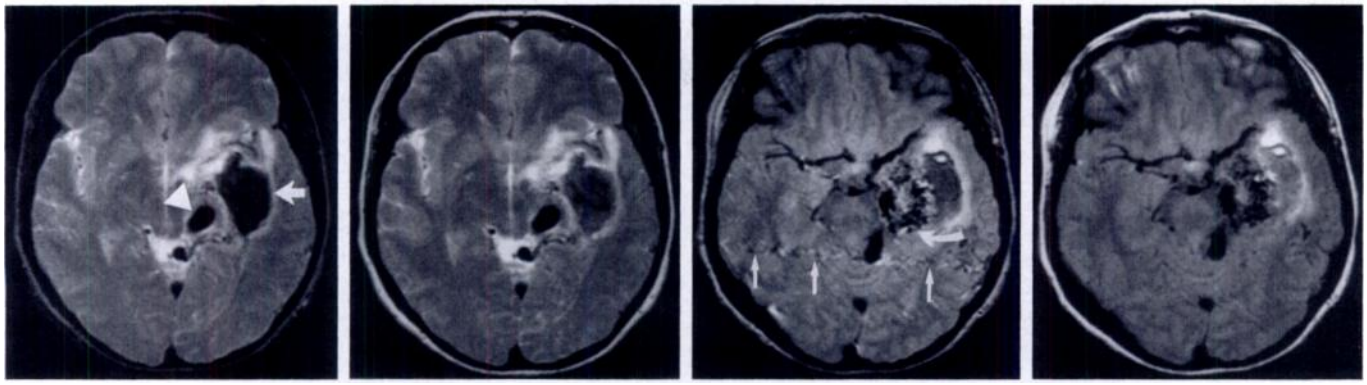

a. b. c. d.

Figure 5. **(a)** Conventional T2-weighted SE image (2,000/80) shows hemorrhage into an arteriovenous malformation (arrow) with a large draining vein (arrowhead). **(b)** FSE image corresponding to that in **a** (2,000/pTE, 80) shows slightly higher signal intensity within the central area of deoxyhemoglobin. **(c)** Conventional PD-weighted SE image (2,000/30) at slightly lower section level demonstrates multiple vessels (curved arrow). Flow-related artifact results from a large draining vein (straight arrows). **(d)** PD-weighted FSE image (2,000/pTE, 16) corresponding to that in **c** at the same level demonstrates no flow-related artifact.

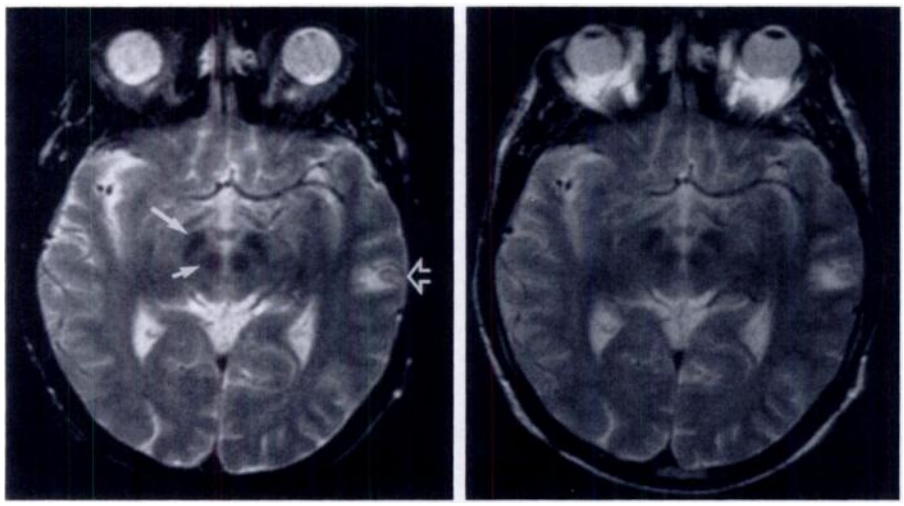

a. b.

Figure 6. **(a)** Red nuclei (short solid arrow) and substantia nigra (long solid arrow) are well seen on conventional SE image (2,000/80). Small hemorrhagic metastasis is also seen (open arrow). **(b)** Corresponding FSE image (2,000/pTE, 80), in which nuclei have slightly higher signal intensity and appear slightly less dark than on the SE image.

ences between FSE and SE T2-weighted image signal intensities for these tissues (see extrapolated values in Table 1). Our results are more in agreement with a recent in vivo study in which larger interecho intervals in SE sequences were shown to have no pronounced effect on the appearance of hemorrhagic lesions (11).

Fat has significantly higher signal intensity ($P < .001$) on FSE images. This probably would not have much effect on diagnostic accuracy in most cases, although an occasional lipoma or other fat-containing lesion could cause diagnostic difficulty. In such cases, fat-suppression methods are available and should be considered for use with FSE imaging. High-intensity fat signal will probably have greater importance in spine studies, where marrow fat usually appears bright on T1-weighted images and darker on T2-weighted images.

Despite the reduced S/N ratios of FSE images, the overall image quality was excellent, and all hemorrhagic foci were identified with both "echoes" of the FSE sequence. S/N measurements are important but provide only one measure of overall image quality. Motion artifact also degrades image quality and, as would be expected with reduced imaging times, was generally less pronounced on FSE images. Also, reduced magnetic susceptibility effects with FSE imaging produce less signal loss adjacent to cortical bone or at interfaces of air with soft tissue. This feature may have advantages in imaging of the paranasal sinuses, skull base, or degenerative spine.

In our study, one prototype FSE sequence was evaluated. The sequence parameters were chosen to match those of typical SE sequences used in clinical practice and to permit comparison of the appearances of blood products on the two types of images. Substantial manipulation of the sequence parameters can produce changes in the appearance and conspicuity of blood products, which is beyond the scope of our study but merits further investigation. Imaging parameters may also be manipulated to provide greater spatial resolution or greater T2 weighting rather than decreased imaging time.

Although the different types of imaging resulted in only slight differences in signal intensity of the various blood products, paramagnetic blood products do appear and measure slightly higher in signal intensity on FSE images. Lesions showed comparable conspicuity in our study, but only a few small or subtle hemorrhagic foci were evaluated (Fig 6), and we have not determined the lower threshold of lesion conspicuity for either method of imaging. It is possible that very small or subtle hemorrhagic foci might be missed with our particular FSE sequence or that a hypointense tumor or other pathologic lesion might be indistinguishable from a small hematoma. FSE images, especially PD-weighted images, are blurrier than their SE counterparts, which is attributable to the use of attenuated, later echoes for the collection of the high-frequency phase-encoding values (2,3). Further work is necessary to determine optimal pulse sequence parameters for visualization and absolute resolution of blood products with FSE imaging.

The categorization of blood products is a complicated topic, and much

research has been performed in the attempt to correlate the biochemical structure of blood breakdown products with appearance on MR images (11–20). With the understanding that pathologic correlation was not possible in this study, we attempted to organize blood products into generally accepted categories. Given the fairly similar appearance of all blood products on FSE and SE images, the precise categorization of blood products probably does not limit our general conclusions.

In summary, although paramagnetic blood products may show greater signal intensity on FSE images, overall contrast and quality with FSE imaging appears comparable with that achieved with SE imaging, and FSE imaging resulted in less motion artifact and nearly identical lesion conspicuity. We conclude that FSE imaging is comparable to conventional dual SE imaging for the evaluation of brain hemorrhage, and the slightly decreased magnetic susceptibility effects seen in our study should not impede the further evaluation of FSE imaging as a rapid, feasible alternative to conventional SE sequences. ■

References

1. Hennig J, Naureth A, Friedburg H. RARE imaging: a fast imaging method for clinical MR. Magn Reson Med 1986; 3:823–833.
2. Mulkern RV, Wong STS, Winalski C, Jolesz FA. Contrast manipulation and artifact assessment of 2D and 3D RARE sequences. Magn Reson Imaging 1990; 8:557–566.
3. Melki PS, Mulkern RV, Panych LS, Jolesz FA. Comparing the FAISE method with conventional dual-echo sequences. JMRI 1991; 1:319–326.
4. Allerhand A. Analysis of Carr-Purcell spin-echo NMR experiments on multiple-spin systems: I—the effect of homonuclear coupling. J Chem Phys 1966; 44:1–9.
5. Gutowsky HS, Vold RL, Wells EJ. Theory of chemical exchange effects in magnetic resonance. J Chem Phys 1965; 43:4107–4125.
6. Bendel P. Spin-echo attenuation by diffusion in nonuniform field gradients. J Magn Reson 1990; 86:509–515.
7. Rozenman Y, Zou X, Kantor HL. Signal loss induced by superparamagnetic iron oxide particles in NMR spin-echo images: the role of diffusion. Magn Reson Med 1990; 14:31–39.
8. Gomori JM, Grossman RJ, Yu-Ip C, Asakura T. NMR relaxation times of blood: dependence on field strength, oxidation state, and cell integrity. J Comput Assist Tomogr 1987; 11:684–690.
9. Twieg DB. The k-space trajectory formulation of the NMR imaging process with applications in analysis and imaging methods. Med Phys 1983; 10:610–621.
10. Kaufman L, Kramer DM, Crooks LE, Ortendahl DA. Measuring signal-to-noise ratios in MR imaging. Radiology 1989; 173: 265–267.
11. Weingarten K, Zimmerman RD, Cahill PT, Deck DFM. Detection of acute intracerebral hemorrhage on MR imaging: ineffectiveness of prolonged interecho interval pulse sequences. AJNR 1991; 12:475–479.
12. Sipponen JT, Sipponen RE, Sivula A. Nuclear magnetic resonance (NMR) imaging of intracranial hemorrhage in the acute and resolving phases. J Comput Assist Tomogr 1983; 7:954–959.
13. DeLaPaz RL, New PFJ, Buonanno FS, et al. NMR imaging of intracranial hemorrhage. J Comput Assist Tomogr 1984; 8:599–607.
14. Gomori JM, Grossman RI, Goldberg HI, et al. Intracranial hematomas: imaging by high-field MR. Radiology 1985; 157:87–93.
15. Cohen MD, McGuire W, Cory DA, Smith JA. MR appearance of blood and blood products: an in vitro study. AJR 1986; 146: 1293–1297.
16. Di Chiro G, Brooks RA, Girton ME, et al. Sequential MR studies of intracerebral hematomas in monkeys. AJNR 1986; 7:193–199.
17. Gomori JM, Grossman RI, Hackney DB, et al. Variable appearances of subacute intracranial hematomas on high-field spin-echo MR. AJNR 1987; 8:1019–1026.
18. Zimmerman RD, Heier LA, Snow RB, et al. Acute intracranial hemorrhage: intensity changes on sequential MR scans at 0.5T. AJNR 1988; 9:47–57.
19. Bradley WG Jr. MRI of hemorrhage and iron in the brain. In: Stark DD, Bradley WG Jr, eds. Magnetic resonance imaging. St Louis: Mosby, 1988; 359–374.
20. Thulborn KR, Brady TJ. Biochemical basis of the MR appearance of cerebral hemorrhage. In: Edelman RR, Hesselink JR, eds. Clinical magnetic resonance imaging. Philadelphia: Saunders, 1990; 255–268.